Low Temperature Physics/Fizika Nizkikh Temperatur, 2019, v. 45, No. 5, pp. 555–561

Percolation transitions in *d*-wave superconductor–half-metallic ferromagnet nanocomposites

V.N. Krivoruchko and V.Yu. Tarenkov

Donetsk Institute for Physics and Engineering of the NAS of Ukraine, 46 Prospect Nauki, Kyev 03028, Ukraine
E-mail: krivoruc@gmail.com

Received October 30, 2018, revised December 13, 2018, published online March 26, 2019

Electrical transport properties of random binary networks composed of high-T_c superconductor $Bi_2Sr_2Ca_2Cu_3O_{6+x}$ microparticles and half-metallic ferromagnet $La_{0.67}Sr_{0.33}MnO_3$ (LSMO) nanoparticles have been investigated. Two resistive percolation transitions (superconductor–metal–semiconductor) have been observed for the nanocomposites with a volume fraction of the LSMO no more than 30%. The nanocomposites basic attributes (transition critical temperatures, current–voltage characteristics, percolation threshold, etc.), most probably, cannot be quantitatively interpreted within the framework of a conventional percolation model. We have explained the observed behavior by a two-level scale interaction in the system caused by (i) a significant geometric disparity between the constituent components and (ii) proximity-induced superconducting state of the half-metallic manganite.

Keywords: nanocomposite, *d*-wave superconductor, half-metallic ferromagnet, resistive percolation transition.

1. Introduction

A common feature of a random insulator–conductor mixture is a sharp increase in an overall conductivity once a critical volume of the conductive phase is reached. This transition is generally interpreted as formation of a cluster of electrically connected conductor particles which spans the entire sample. This picture implies a power-low behavior of the conductivity in the vicinity of the percolation transition [1–3]. However, in the more general cases with a variable coupling strength or few-level scales characterizing different geometrical lengths, the conductivity behavior may be non-universal [4–6]. When indirect interaction between the constituents exists or additional degrees of freedom become available, this leads to a new or non-universal behavior of the composite system. An example is electrical percolation transitions in a system where a superconductor and a ferromagnetic metal are counterpartners. In this case, percolation effects can be more complicated as far as the electrical coupling between constituent components can be both direct, geometric contact, and indirect one, via spin-dependent proximity effects. Hybrid half-metallic ferromagnet (hmF)–superconductor (SC) random composite structures can enable new intelligently tailored functionality and have gained attention over the past few years as new functional materials [4,7–10].

A special case is hmF–SC *nano*composites. Here, due to proximity effects, there are many important issues beyond the conventional percolation theory [1–3]. The point is that for nanoparticles the geometric contacts and electrical connectivity of individual particles are often not the same [11,12]. So far, a few works have been reported on investigations of transport properties of a SC with half-metallic magnetic nanoparticles composites. Unconventional double percolation transition is identified in Ref. 4 for a binary network composed of nanoparticles of MgB_2 and CrO_2. Here the double percolation transition (superconductor–insulator–metal) was especially pronounced at liquid helium temperatures. It is controlled by the components volume fractions and originates from the suppressed interface conduction and tunneling as well as a large geometric disparity between particles [4]. Acharya *et al*. [9] prepared and studied electrical transport characteristics of $Bi_2Sr_2CaCu_2O_8/BiFeO_3$ nanocomposite with various weight percentage of $BiFeO_3$ nanoparticles ($BiFeO_3$ in nanoform is insulating and exhibits superparamagnetism). Measurement of the critical current density reveals that the superconducting transition temperature splits into two, T_{c1} and T_{c2}, along with a broadening of overall superconducting transition. Authors accounted such behavior to the weak-link nature of a granular SC as the latter is composed of superconducting grains embedded in a nonsuperconducting host. Of the two superconducting transitions temperatures, the higher one, T_{c1}, marks the superconductivity in grains whereas the grain boundary still remains normal, and the lower one, T_{c2}, emerges when the grain boundary also becomes superconducting. The appearance of additional transition temperature and its broadening

clearly reflects that $BiFeO_3$ goes to the grain boundary region and becomes superconducting only due to the proximity effect at lower temperatures [9].

In this paper, we report on the results of experimental investigations of electrical percolation transitions in random binary nanocomposites, which have been composed of cuprate SC $Bi_2Sr_2Ca_2Cu_3O_{6+x}$ (Bi2223) microparticles and hmF $La_{0.67}Sr_{0.33}MnO_3$ (LSMO) nanoparticles. Namely, we designed and fabricated a number of random nanocrystalline samples by combining with different volume ratios the hmF and *d*-wave SC components. This allowed us to investigate the percolation effects in electrical transport characteristics of the nanocomposites. An unusually large value of the concentration threshold for Bi2223 is detected for the realization a double percolation transition superconductor–metal–semiconductor. We argue that the observed behavior is due to two different length scales of effective interaction in the system and is specified by: (i) a significant geometric disparity between the constituent particles and (ii) an unconventional (most probably, triplet) superconducting state induced in the nanocomposite by spin-dependent superconducting proximity effect [13].

The structure of the paper is as follows. Section 2 is devoted to the experimental details. Section 3 is a central one. To obtain a reference data, we start with measurements of the resistance temperature dependences for compacted samples of pure Bi2223 microparticles and LSMO nanoparticles (Sec. 3.1). In Secs. 3.2 and 3.3, the electrical transport characteristics of the nanocomposites are presented at above and below the metal–semiconductor transition temperature, respectively. We discuss the experimental results in the context of a two-level percolation process in the hmF:SC random nanocomposite, along with a splitting of overall superconducting transition. We finalize with the Conclusion (Sec. 4).

2. Methods of preparation and samples

A series of nanocomposite samples have been fabricated. The composites are prepared by mixing the cuprate *d*-wave SC Bi2223 ($Bi_2Sr_2Ca_2Cu_3O_{6+x}$, the superconducting transition temperature in the interval T_c = 100–110 K) and the manganite LSMO ($La_{0.67}Sr_{0.33}MnO_3$, the Curie temperature $T_C \approx 360$ K of monocrystalline samples) with a different volume content of the components. A specific feature of the composites is that the high-T_c SC is used a powder with a grain size of 5–15 μm, while the manganite LSMO is a nanopowder with a particle size of 20–30 nm. Note that the coherence length of Bi2223 is anisotropic with $\xi_{ab}(0) \approx 2$ nm in the *ab* plane, which is a typical value for cuprate oxides, and along the *c*-axis direction $\xi_c(0)$ is less than 0.02 nm. Hence, the size of the Bi2223 grains was much larger than the superconducting coherence length.

Details of the LSMO nanoparticle preparation can be found in Refs. 14, 15. Magnetization measurements, in particular, the nuclear magnetic resonance and the nuclear spin-spin relaxation of ^{55}Mn nuclei of nanopowders and polycrystalline samples of the same composition confirmed that manganite nanoparticles of such sizes retain their magnetic properties and the double exchange mechanism of magnetic interaction (and thus, half-metallic properties) [16,17].

The samples were prepared by using a traditional cold-pressed technique. The raw materials were mixed according to their volume ratios. A homogeneous composition was achieved by mixing the components in alcohol, followed by drying and an additional mechanical mixing at temperature above the Curie to avoid magnetic coupling of the manganite nanoparticles. Plates with dimensions 1×0.2×10 mm were then compacted at pressures up to P = = 40–60 kbar from the resulting mixture. Such pressure provides a good electrical connection between the grains and high mechanical strength of the plate. The samples were not subjected to sintering in order to avoid interdiffusion and chemical reaction between the components. Four contacts for current and potential measurements were formed by introducing fine silver paste to the designated contact region on the plate. Samples of different compositions were prepared according to the volume fraction, percentagewise, of the components LSMO:Bi2223 = = 0:100, 10:90, 20:80, 25:75, 30:70, 40:60, 50:50, 100:0. Inset in Fig. 1 sketches out the nanocomposite obtained structure.

The current–voltage (*I–V*) characteristics were measured by using a conventional four-terminal technique. Resistivity as a function of temperature was measured directly by using an ac voltage bias source with a small output resistance and ~ 400 μV amplitude of the signal on the sample. We measured electrical transport characteristics of the samples and studied the percolation transition dependence on the sample's composition.

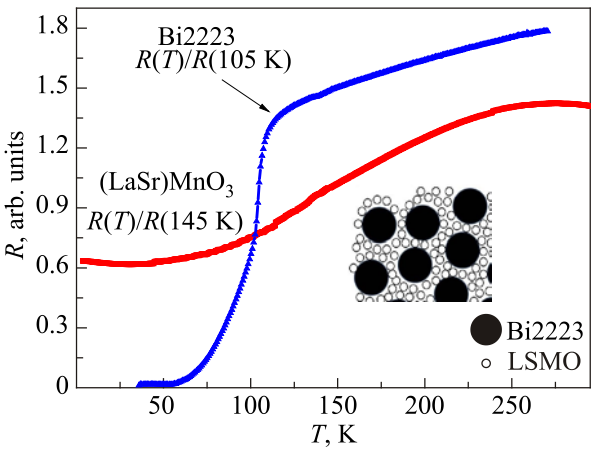

Fig. 1. Resistivity-*vs*-temperature dependences for pure compacted samples of Bi2223 microparticles and LSMO nanoparticles. Inset: sketch of the nanocomposite structure.

3. Results and discussions

3.1. Pure compacted samples

The Bi–Sr–Ca–Cu–O system is known to have three types of structures, namely $Bi_2Sr_2Cu_2O_{6+x}$ (Bi2223), $Bi_2Sr_2CaCu_2O_{6+x}$ (Bi2212) and $Bi_2Sr_2Cu_2O_{6+x}$ (Bi2201), which have the critical temperature T_c of about 100, 85 and 20 K, respectively. No more than 15% of residual secondary phase Bi2212 has been detected in our compacted Bi2223 samples by x-ray diffraction studies. Note, that the residual Bi2212 phase localizes, mainly, at grain boundaries of the Bi2223 phase [18].

The temperature behavior of the pure compacted Bi-2223 sample resistivity, $R(T)$, is shown in Fig. 1. As seen in the figure, the superconducting transition of the compacted Bi2223 is in the interval 65–100 K and $R(T)$ dependence contains two decreasing segments which correspond to Bi2223 and Bi2212 transitions to a superconducting state. This points that a granular structure of the sample does not affect a global sample superconductivity. The superconducting state is consolidated at ~ 65 K. Accordingly, the compacted Bi2223 samples contain transparent interfaces and strong links among grains. Above T_c, the sample is a good conductor with low resistivity.

The LSMO sample's zero-field $R(T)$ characteristic is shown in Fig. 1, as well. It demonstrates a metal–semiconductor transition at $T_p \approx 280$ K (for bulk LSMO $T_p \approx$ ≈ 360 K [19]) and a metallic behavior at low temperature. Figure 2 illustrates the LSMO sample magnetoresistive characteristics. The low-field ($H \approx 1$ kOe) magnetoresistive effect $[\rho(T,0) - \rho(T,H)]/\rho(T,0)$ at $T = 77$ K was about 10%. This suggests that the contribution of inter granular junctions to the total sample resistance is relatively small and confirms high quality of the nanoceramic LSMO sample. We find it convenient to describe the LSMO $R(T)$ behavior in terms of the magnetic polaron picture [20]. The main assumption of the theory [20] is that it does not demand the existence of an abrupt metal–insulator transition in doped manganites. Instead, the theory predicts the coexistence of two electronic processes: (i) energy-conserving tunneling process and (ii) thermally assisted hopping process. Both processes are temperature dependent and, with increasing temperature, the probability of tunneling process decreases, while the probability of hopping process increases. At intermediate temperature, near the $R(T)$ peak, the hopping process overgrows the tunneling one and the sample behaves as an insulator (semiconductor) at higher temperatures. The peak temperature T_p should not coincide with the Curie temperature T_C, nevertheless, it correlates with the T_C since they both are dependent on the number of thermal magnons.

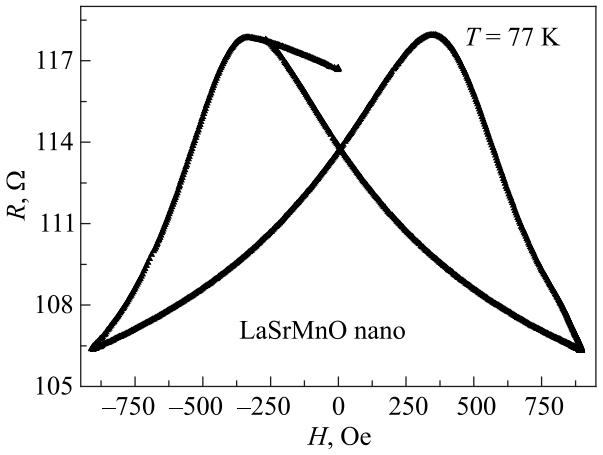

Fig. 2. Compacted LSMO sample low-field magnetoresistive effect; $T = 77$ K.

3.2. Composites' transport characteristics at $T > T_p$

Let us start the discussion of the composite transport characteristics at temperatures when LSMO behaves as an insulator and we deal with random insulator–conductor mixtures. Figure 3 shows the dependence of the LSMO:Bi2223 nanocomposite resistivity $R(T)$ on the volume content of LSMO at $T = 300$ K. A rapid change in the sample's resistivity occurs in the vicinity of about 20 vol.% of LSMO. As we see (left, logarithmic, axis in Fig. 3), as Bi2223 grains are sufficiently decoupled, at fixed temperature the resistance is controlled by a tunneling process and is given by

$$R = R_0 \exp(r_{ij}/\zeta). \quad (1)$$

Here $R_0 = R(V_{LSMO} = 0)$ is a constant (or a weak function of the LSMO volume content), ζ is the characteristic tunneling length, and is r_{ij} is the minimal distance between the two Bi2223 particles.

As is known (see, e.g., [3]), the electrical conductivity of a composite generated on a mechanical mixture of the components is determined by the structure of the conduc-

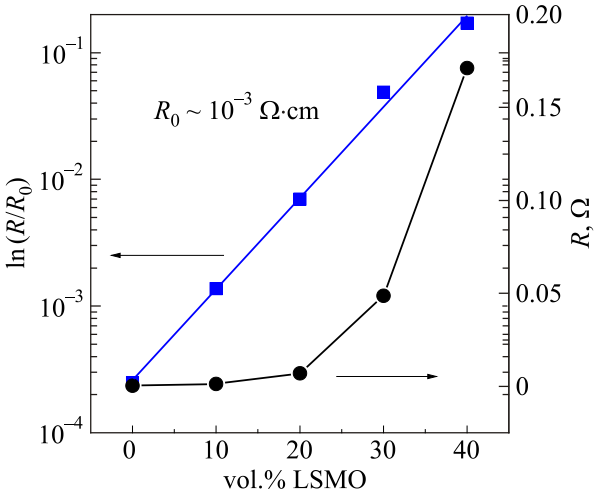

Fig. 3. Dependence of the LSMO:Bi2223 nanocomposite resistivity $R(T)$ on the volume content of LSMO; $R_0 = R(V_{LSMO} = 0)$, $T = 300$ K.

tive percolation cluster arising in the system. If an infinite percolation cluster for a highly conductive phase is broken, transport properties of the composite are determined by a high-resistive ingredient. In our case, the choice of Bi2223 as a matrix is justified by a high conductivity of the compacted Bi2223 powder, as well as its well pronounced metallic behavior indicating clean grain boundaries of Bi2223. Since electron mean free path in manganite oxides is quite small [19], we can assume that the electron transport is of the diffusive type. Thus, in our case, the high-resistive component is LSMO manganite. We find that the nanocomposites resistance behavior on the LSMO concentration, $R(V_{LSMO})$ Eq. (1), is compatible with the tunneling-percolation model [5]. According to the approach [5], in the intermediate regime between the percolation-like and the hopping-like electronic processes the tunneling between particles is a continuous function of the interparticle distances. Correspondingly, the resulting tunneling conductance of a nanocomposite decays exponentially with these distances and does not imply any sharp cutoff or threshold.

Significant deviation of $R(V_{LSMO})$ from the conventional percolation theory, which predicts a power-law behavior of the conductance [3], we ascribe to a large geometric disparity between the components and a polaron-type conductivity of half-metallic manganites. As it follows from Fig. 3, already 30 vol.% of the LSMO nanoparticles coat the Bi2223 grains surface, preventing direct contact between them (see inset in Fig. 1). As a result, the resistance of the composite is determined by the current flowing through the –Bi2223–LSMO–Bi2223-channels. Above T_p this leads to a hopping-like regime in the nanocomposite's electrical conductivity. Therefore, the metal–semiconductor transition is a continuous function of the nanoparticles concentration and does not demonstrate a sharp cutoff or a percolation threshold.

3.3. Composites' transport characteristics at $T < T_p$

The temperature dependences of the nanocomposites resistivity $R(T)$ below T_p are shown in Fig. 4 for 20, 25, 30, 40, and 50 vol.% of LSMO. As seen in the figure, the addition of already 20 vol.% of LSMO significantly broadens the resistive superconducting transition $R(T)$ of the nanocomposite. The resistance of the sample with 40 vol.% of LSMO nanoparticles remains finite in all investigated temperature range, although the onset of the $R(T)$ reduction matches the T_c of Bi2223.

Figure 5 illustrates the I–V characteristic of the samples with 20, 25, and 30 vol.% of LSMO taken at 4.2 K. We observe a clear zero-resistance supercurrent branch, with an excess current I_{exc} of 0.32, 0.27, and 0.12 mA, respectively. The presence of ferromagnetic LSMO nanoparticles causes the formation of weak links at the grain's boundaries, as well as a local magnetic field of the hmF particles certainly limits the critical current density in the nanocomposite [21].

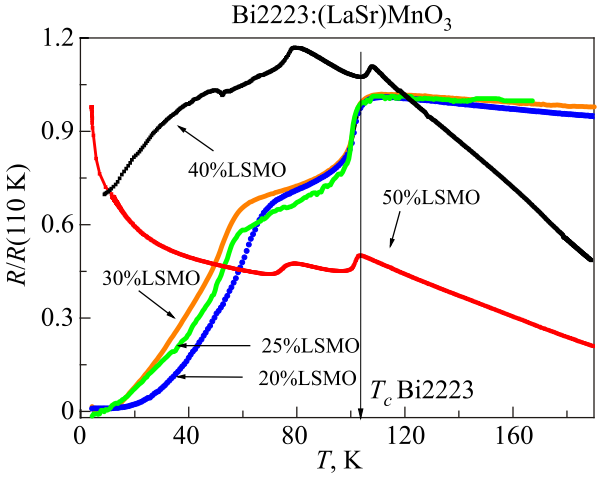

Fig. 4. (Color online) Temperature dependences of the nanocomposite's resistivity with the volume fraction, percentagewise, 20, 25, 30, 40, and 50 vol.% of the LSMO.

As it follows from $R(T)$ characteristics, Fig. 4, the superconducting transition temperature splits into two, T_{c1} and T_{c2}, along with a broadening of overall superconducting transition. The higher temperature, T_{c1}, marks the superconductivity of Bi2223 grains whereas the grain boundary still remains normal. The lower one, T_{c2}, appears when the grain boundary becomes superconducting as well. One of the possible origins of the second superconducting transition is the presence of the additional phases Bi2212 which has the critical temperature of about 80 K. Another possibility is the unconventional superconducting state (a mixture of singlet and triplet correlations) induced in the nanocomposite.

Superconductivity in bulk composite systems was extensively studied within the percolation scenario [4,8,9,11,12]. It has been established that when grains of the superconducting material, d, are large enough, $d >> \xi_S$, their basic intra-granular characteristics (critical temperature, gap value, etc.) are not affected by the proximity of the non-

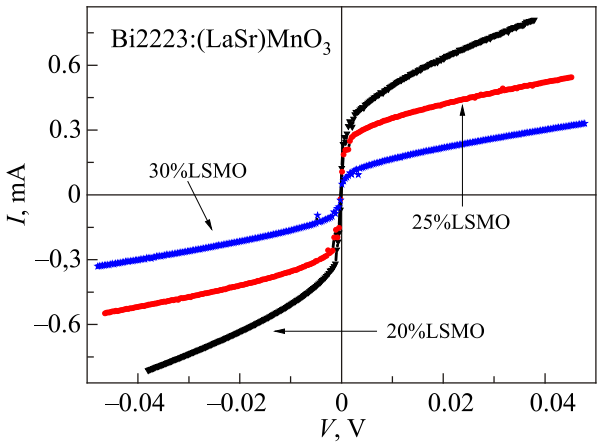

Fig. 5. (Color online) Current–voltage characteristics for the nanocomposites with 20, 25, and 30 vol.% of LSMO at 4.2 K.

superconducting component and remain close to the bulk value both above and below the percolation threshold. For a three-dimensional composite with roughly the *same geometrical size* of components, the three-dimensional lattice percolation model predicts $f_C = 0.16 \pm 0.02$ for the percolation threshold of the volume fraction, f, of a superconducting component (i.e., f_C being a percolation threshold of grains with linear dimension $\gtrsim \xi_S$). Thus, for the composite systems under consideration with the large enough grains of the superconducting material, below the percolation threshold the macroscopic transition temperature T_c should not be strongly dependent on the contents variation. However, as it is seen in Fig. 4, even for the sample with volume fraction about $f = 0.5$, i.e., about three times larger than the conventional percolation model predicts, there is no transition into a superconducting state. Moreover, the transition temperature T_c is strongly reduced even at concentrations when an infinite percolating cluster of Bi2223 constitutes: see $R(T)$ data in Fig. 4 for the samples with 20, 25, and 30 vol.% of LSMO (80, 75, and 70 vol.% of the superconducting component). Thus, the predictions based on the conventional percolation model do not work for the Bi2223:LSMO nanocomposites, most probably, due to two factors: (i) unconventional proximity effect and (ii) essential difference in geometrical size of the components.

As is known, below a superconducting transition an indirect (via proximity effect) coupling between constituent components, SC and hmF, enters into a force. From a theoretical viewpoint [13,22–24], the appearance of a long-range proximity effect can be realized if there is a spatial variation of the magnetization at the ferromagnet surface. In this case, the spin conservation low is not fulfilled and a triplet component of anomalous correlations should be taken into consideration. A characteristic coherence length of triplet correlations $\xi_F = (D_F/2\pi T)^{1/2}$ can be as large as ~ 100 nm at low temperatures (here D_F is the diffusivity of the ferromagnet metal and T is the temperature; we choose $h = k_B = 1$). In previous papers, anomalous superconductivity has been detected in nanocomposites MgB_2:$La_{0.67}Sr_{0.33}MnO_3$ [25] and MgB_2:$La_{0.7}Ca_{0.3}MnO_3$ [10], as well as in half-metallic manganite, (La,Sr)MnO_3 and (La,Ca)MnO_3, being in contact with an *s*-wave SC, Pb or MgB_2 [26–28]. It was argued that at low-temperatures manganites are thermodynamically very close to a superconducting state with a triplet *p*-wave even frequency pairing. Being proximity coupled to the singlet SC, the $m = 0$ triplet component in the manganite is coupled via the boundary condition to the singlet pairing amplitude in the SC partner. At the same time, the spin-active boundary leads to coupling of the $m = 0$ triplet component with an equal-spin, $m = 1$, pairing amplitude in manganite. These couplings yield phase coherency of both the $m = 0$ and equal-spin m = 1 triplet Cooper pairs in the hmF with a large quasiparticle gap [29].

Thus, in the case of the nanocomposite under consideration, proximity effect possesses a several specific peculiarities. Firstly, because the contacts between Bi2223 grains are through the half-metallic LSMO *nano*grains, this causes a significant broadening of the nanocomposites transition to a superconducting state. The dependence of the superconducting properties on the exchange field inhomogeneity is expected to be a general feature of the proximity effect in mesoscopic F–SC structures [13,24]. Secondly, high-T_c superconductors are widely believed to have a dominant *d*-wave pairing symmetry [30]. As theory predicts and experiment provides evidences (see, e.g., [13,24,31–36]), in proximity coupled *d*-wave SC/ferromagnet structures an unconventional (spin-triplet) superconducting state can be generated. This also means the appearance of a new geometrical length which characterizes unconventional superconducting state (a mixture of *d*-wave singlet and *p*-wave triplet Cooper pairs) induced in the nanocomposite. To date, we know of no reports addressing the scenario for anomalous superconductivity of high-T_c *d*-wave SC–hmF nanocomposites and proximity effects in such type of nanocomposites.

4. Conclusion

Unconventional superconducting state induced in a hmF by *d*-wave SC bears a great fundamental interest and can be useful for future applications in superconducting spintronics (see, e.g., [37] and references therein). Traditional search of materials for superconducting spintronics have mainly focused on multilayers and engineering of interfaces between SC and ferromagnetic materials. The aim is to find the ways to enhance the triplet state critical temperature and to generate a long-ranged spin-triplet state. Yet, in our opinion, there are other ways to produce materials demonstrating long-ranged spin-triplet correlations. A direct coupling of high-temperature superconducting and magnetic orders can be possible through a creation of the spin-triplet Cooper pairs in nanocomposite materials.

In summary, we have studied random nanocomposites of a half-metallic ferromagnet and a high-temperature superconductor with different volume fractions and a large geometrical disparity: nanoparticles of $La_{0.67}Sr_{0.33}MnO_3$ and microparticles of $Bi_2Sr_2Ca_2Cu_3O_{6+x}$. We have investigated transport characteristics of the nanocomposites and, in particular, a superconducting percolation transition arising through contacts between the components. It was found that the classical percolation theory is strongly affected by both a large geometrical disparity between components and by the proximity effect. Double resistive percolation transition (superconductor–metal–semiconductor) has been observed for nanocomposites with the volume fraction of LSMO below 30%. The observed behavior is due to two different effective length scales which reflect a two-level scale interaction in the system. One is determined by a geometric difference between constituent components, whereas the another arises due to proximity effect. We have argued

that the constituent particle geometrical size and indirect interaction via proximity effect play a crucial role in achieving conditions enabling the percolation transitions in the nanocomposites under consideration. The unusual transport properties of this type nanocomposites bear great fundamental interest and make their promise for applications, e.g., as novel functional materials.

Acknowledgments

The authors are grateful to I. Danilenko and O. Gorban' for the preparation of manganite nanoparticles, and A.D. Rud' for x-ray diffraction measurements. We also thank M.A. Belogolovskii for fruitful discussions. The work was supported by the supported by the Science and Technology Center in Ukraine and the National Academy of Sciences of Ukraine (project No: 6250).

1. S. Kikpartrick, *Rev. Mod. Phys*. **45**, 574 (1973).
2. A. Bunde and W. Dieterich, *J. Electroceram*. **5**, 81 (2000).
3. I. Balberg, *J. Phys. D: Appl. Phys*. **42**, 064003 (2009).
4. X. Liu, R. P. Panguluri, Z.-F. Huang, and B. Nadgorny, *Phys. Rev. Lett.* **104**, 035701 (2010).
5. G. Ambrosetti, C. Grimaldi, I. Balberg, T. Maeder, A. Danani, and P. Ryser, *Phys. Rev. B* **81**, 155434 (2010).
6. J. Li, B. Ray, M.A. Alam, and M. Östling, *Phys. Rev. E* **85**, 021109 (2012).
7. Z. Rubin, S.A. Sunshine, M.B. Heaney, I. Bloom, and I. Balberg, *Phys. Rev. B* **59**, 12196 (1999).
8. Y.M. Strelniker, A. Frydman, and S. Havlin, *Phys. Rev. B* **76**, 224528 (2007).
9. S. Acharya, A. K. Biswal, J. Ray, and P. N. Vishwakarma. *J. Appl. Phys.* **112**, 053916 (2012).
10. V.V. Kononenko, V.Yu. Tarenkov, A.I. Dyachenko, and V.N. Varukhin, *Fiz. Nizk. Temp*. **41**, 262 (2015) [*Low Temp. Phys*. **41**, 199 (2015)].
11. I. Sternfeld, V. Shelukhin, A. Tsukernik, M. Karpovski, A. Gerber, and A. Palevski, *Phys. Rev. B* **71**, 064515 (2005).
12. L. Ruiz-Valdepeñas, M. Vélez, F. Valdés-Bango, L.M. Álvarez-Prado, J.I. Martín, E. Navarro, J.M. Alameda, and J.L. Vicent, *New J. Phys*. **15**, 103025 (2013).
13. M. Eschrig and T. Löfwander, *Nature Phys*. **4**, 138 (2008).
14. M.M. Savosta, V.N. Krivoruchko, I.A. Danielenko, V.Yu. Tarenkov, T.E. Konstantinova, A.V. Borodin, and V.N. Varyukhin, *Phys. Rev. B* **69**, 024413 (2004).
15. V. Krivoruchko, T. Konstantinova, A. Mazur, A. Prokhorov, and V. Varyukhin, *J. Magn. Magn. Mater*. **300**, e122 (2006).
16. A.S. Mazur, V.N. Krivoruchko, and I.A. Danilenko, *Fiz. Nizk. Temp.* **33**, 1227 (2007) [*Low Temp. Phys.* **33**, 931 (2007)].
17. A.N. Ulyanov, D.S. Yang, A.S. Mazur, V.N. Krivoruchko, G.G. Levchenko, I.A. Danilenko, and T.E. Konstantinova, *J. Appl. Phys*. **109**, 123928 (2011).
18. H. Deng, P. Hua, W. Wang, C. Dong, H. Chen, F. Wu, H. Wang, Y. Zhou, and G. Yuan, *Physica C* **339**, 181 (2000).
19. E. Dagotto, T. Hotta, and A. Moreo, *Phys Rep.* **344**, 1 (2001).
20. S. Zhang. *J. Appl. Phys.* **79**, 4542 (1996).
21. O. Paredes, E. Baca, and O. Morán, *J. Supercond. Nov. Magn.* **26**, 2323 (2013).
22. F.S. Bergeret, A.F. Volkov, and K.B. Efetov, *Phys. Rev. Lett*. **86**, 4096 (2001).
23. A. Kadigrobov, R.I. Shekhter, and M. Jonson, *Europhys. Lett.* **54**, 394 (2001).
24. M. Eschrig, J. Kopu, J.C. Cuevas, and G. Schön, *Phys. Rev. Lett.* **90**, 137003 (2003).
25. V.N. Krivoruchko and V.Yu. Tarenkov. *Phys. Rev. B* **86**, 104502 (2012).
26. V.N. Krivoruchko, V.Yu. Tarenkov, A.I. D'yachenko, and V.N. Varyukhin, *Europhys. Lett.* **75**, 294 (2006).
27. V.N. Krivoruchko and V.Yu. Tarenkov, *Phys. Rev. B* **75**, 214508 (2007).
28. V.N. Krivoruchko and V.Yu. Tarenkov, *Phys. Rev. B* **78**, 054522 (2008).
29. V.N. Krivoruchko, A.I. D'yachenko, and V.Yu. Tarenkov, *Fiz. Nizk. Temp.* **40**, 1147 (2014) [*Low Temp. Phys*. **40**, 895 (2014)].
30. C.C. Tsuei and J.R. Kirtley, *Rev. Mod. Phys*. **72**, 969 (2000).
31. Z.P. Niu and D.Y. Xing, *Phys. Rev. Lett*. **98**, 057005 (2007).
32. W. Wang, D.F. Shao, R.C. Xiao, W.J. Lu, and H.Y. Wu, *J. Supercond. Nov. Magn*. **29**, 1741 (2016).
33. T. Hu, H. Xiao, C. Visani, Z. Sefrioui, J. Santamaria, and C.C. Almasan, *Phys. Rev. B* **80**, 060506(R) (2009).
34. K. Dybko, K. Werner-Malento, P. Aleshkevych, M. Wojcik, M. Sawicki, and P. Przyslupski, *Phys. Rev. B* **80**, 144504 (2009).
35. Y. Kalcheim, T. Kirzhner, G. Koren, and O. Millo, *Phys. Rev. B* **83**, 064510 (2011).
36. D.K. Satapathy, M.A. Uribe-Laverde, I. Marozau, V.K. Malik, S. Das, Th. Wagner, C. Marcelot, J. Stahn, S. Brück, A. Rühm, S. Macke, T. Tietze, E. Goering, A. Frañó, J.-H. Kim, M. Wu, E. Benckiser, B. Keimer, A. Devishvili, B.P. Toperverg, M. Merz, P. Nagel, S. Schuppler, and C. Bernhard, *Phys. Rev. Lett*. **108**, 197201 (2012).
37. J. Linder and J.W.A. Robinson, *Nature Phys*. **11**, 307 (2015).

Перколяційні переходи у нанокомпозитах *d*-хвильовий надпровідник–феромагнітний напівметал

Досліджено електричні транспортні властивості хаотичних двокомпонентних структур, складених з мікрочастинок високотемпературного надпровідника $Bi_2Sr_2Ca_2Cu_3O_{6+x}$ та наночастинок напівметалевого феромагнетика $La_{0,67}Sr_{0,33}MnO_3$ (LSMO). Для нанокомпозитів з об'ємним складом LSMO не більше ніж 30% спостерігалися два резистивних перколяційних переходи (надпровідник–метал–напівпровідник). Основні характеристики нанокомпозитів (критичні температури переходів, вольт-амперні характеристики, поріг перколяційних переходів і т.п.), найбільш ймовірно, не можуть бути кількісно описані у рамках стандартної перколяційної моде-

лі. Пояснено поведінку, що спостерігається, двома різними характерними масштабами взаємодії в системі, що обумовлено (i) істотною геометричною різницею її компонент та (ii) наведеним ефектом близькості надпровідним станом напівметалевого манганіту.

Ключові слова: нанокомпозит, *d*-хвильовий надпровідник, напівметалевий феромагнетик, резистивні перколяційні переходи.

Перколяционные переходы в нанокомпозитах *d*-волновой сверхпроводник–ферромагнитный полуметалл

В.Н. Криворучко, В.Ю. Таренков

Исследованы электрические транспортные свойства хаотических двухкомпонентных структур, составленных из микрочастиц высокотемпературного сверхпроводника $Bi_2Sr_2Ca_2Cu_3O_{6+x}$ и наночастиц полуметаллического ферромагнетика $La_{0,67}Sr_{0,33}MnO_3$ (LSMO). Для нанокомпозитов с объемным составом LSMO не более 30% наблюдались два резистивных перколяционные перехода (сверхпроводник–металл–полупроводник). Основные характеристики нанокомпозитов (критические температуры переходов, вольтамперные характеристики, порог перколяционных переходов и т.п.), наиболее вероятно, не могут быть количественно описаны в рамках стандартной перколяционной модели. Наблюдаемое поведение объяснено двумя различными характерными масштабами взаимодействия в системе, что обусловлено (i) существенной геометрической разницей ее компонент и (ii) индуцированным эффектом близости сверхпроводящим состоянием полуметаллического манганита.

Ключевые слова: нанокомпозит, *d*-волновой сверхпроводник, полуметаллический ферромагнетик, резистивные перколяционные переходы.